OXFORD

Journal of Petrology, 2024, **65**, egae033
https://doi.org/10.1093/petrology/egae033
Advance access publication date 28 March 2024
Letter

Fluoritites Produced by Crystallization of Carbonate–Fluoride Magma

Aleksandr S Stepanov[1]*, Jovid Aminov[2,3], Sharifjon Odinaev[3,4], Farukh Sh Iskandarov[5], Shao-Yong Jiang[1] and Nikolai S Karmanov[6]

[1]State Key Laboratory of Geological Processes and Mineral Resources, Collaborative Innovation Center for Exploration of Strategic Mineral Resources, School of Earth Resources, China University of Geosciences, Wuhan 430074, China
[2]Department of Earth and Environmental Sciences, University of Central Asia, 736000 Khorog, Tajikistan
[3]Institute of Geology, Earthquake Engineering and Seismology, National Academy of Sciences of Tajikistan, Dushanbe, 734063, Tajikistan
[4]State Key Laboratory of Isotope Geochemistry, Guangzhou Institute of Geochemistry, Chinese Academy of Sciences, Guangzhou, China
[5]Department of Mineralogy and Petrography, Tajik National University, Dushanbe 734025, Tajikistan
[6]V.S. Sobolev Institute of Geology and Mineralogy, Siberian Branch of the Russian Academy of Sciences, pr. Akademika Koptyuga 3, Novosibirsk 630090, Russia
*Corresponding author. State Key Laboratory of Geological Processes and Mineral Resources, Collaborative Innovation Center for Exploration of Strategic Mineral Resources, School of Earth Resources, China University of Geosciences, Wuhan 430074, China. E-mail: aleksandr@cug.edu.cn

Fluorite-dominated rocks are occasionally found in association with carbonatites, but their geologic and petrologic relations are rarely reported. The Dunkeldyk area of the Pamir mountains in south-eastern Tajikistan contains dikes of distinctive rocks composed of calcite, fluorite, celestine-barite, sulfides, apatite, with minor quartz, biotite, and REE fluorcarbonates. The dikes have sharp contacts with the host (meta-)sedimentary rocks and layering with ribbons, ranging from fluorite-bearing calcite carbonatites to fluoritites (rocks with >50% fluorite). The fluoritites are characterized by high Ca, F, Ba, Sr, REE, and S coupled with anomalously low O. The geologic relations and textures suggest a magmatic origin of the dikes from melts close to calcite–fluorite eutectic that experienced nucleation-controlled differentiation during the crystallization of dikes and the formation of fluoritite cumulates in larger intrusions. The Dunkeldyk dikes demonstrate that sizable geological bodies of fluorite-dominated rocks could form from carbonate–fluoride melts originating from the differentiation of alkaline silicate magmas.

Key words: fluoritite; fluorite; carbonatite; REE; alkaline magma

INTRODUCTION

Magmatism on the Earth is dominated by silicate liquids. However, less common sulfide and carbonate melts attract a lot of attention due to their economic significance and anomalous geochemical properties. Experimental data suggest that fluoride and carbonate–fluoride melts could exist at conditions relevant to terrestrial magmatic systems (Veksler *et al.*, 2005, 2012; Chebotarev *et al.*, 2018; Yang & van Hinsberg, 2019), yet the evidence of such melts in the crust remains tentative. Products of crystallization of fluoride-rich melts have been observed as aggregates of F-rich minerals in topaz-bearing felsic rocks (Peretyazhko *et al.*, 2007), peralkaline granites (Vasyukova & Williams-Jones, 2016), and calcite–fluorite aggregates (Kynicky *et al.*, 2019). Fluoride-rich melt inclusions have been discovered in the peralkaline granite of the Strange Lake pluton, Canada (Vasyukova & Williams-Jones, 2016). The findings of fluid inclusions in fluorite-rich rocks led to interpretation of crystallization of these rocks from hydrous fluids and in magmatic-hydrothermal processes (Redina *et al.*, 2020, 2021). While these observations demonstrate that fluoride-rich melts could form during the late stages of silicate and carbonate magma crystallization, the existence and appearance of rocks produced by such melts remain enigmatic. Rocks with high fluorite content, commonly associated with carbonatites, have been observed in multiple locations (Table 1) and are particularly well known in Central Italy (Stoppa *et al.*, 2016). However, the geology, petrography, and geochemistry of these rocks are rarely characterized in detail.

Here, we describe dikes from the Dunkeldyk, south-eastern Pamir, Tajikistan, containing significant portion of fluorite-dominated rocks. We propose dikes crystallization from carbonate–fluoride melts and offer a new mechanism for the formation of orthomagmatic fluorite-dominated rocks.

GEOLOGICAL SETTING

The Pamir plateau comprises three main terranes: the Northern, Central, and Southern Pamir (Fig. 1A). While the Northern Pamir is of Laurasian-Asian affinity, the Central and Southern Pamir represent parts of the Gondwana accreted to the southern margin of Eurasia (Angiolini *et al.*, 2013). The Cenozoic India-Asia collision intensively deformed, uplifted, and thickened the Pamir terranes (Stubner *et al.*, 2013). The oldest igneous rocks of the Southern Pamir are late Triassic to early Jurassic, related to the closure of the Mesotethys ocean (Yogibekov *et al.*, 2023). During the early Cretaceous, northward flat-slab subduction of the Neotethys oceanic crust led to widespread arc-related magmatism (Aminov *et al.*, 2017; Chapman *et al.*, 2018). In the early Miocene, the gravitational instability of the overthickened crust of the Pamir triggered

Received: January 26, 2024. **Revised:** March 14, 2024. **Accepted:** March 26, 2024

Table 1: Summary on localities, where fluorite-rich rocks related to carbonatite magmatism have been reported

Locality	Description	References
Eldor carbonatite, Canada	Fluorite-rich rocks associated with carbonatites	Beland & Williams-Jones (2021)
Grenville Province, Canada	Fluorite–apatite–calcite veins	Lentz (1991)
Daluxiang, China	Fluorite-rich rocks associated with carbonatites	Xu *et al.* (2008)
Maoniuping, China	Fluorite-rich rocks associated with carbonatites	Xu *et al.* (2008)
Bayan Obo, China	Fluorite-rich rocks associated with carbonatites	Xu *et al.* (2008)
Pianciano, Italy	Volcanic and hypabyssal rocks with fluorite, fluoritites	Stoppa *et al.* (2016)
Ruri dikes, Kenya	Fluorite-rich rocks associated with carbonatites	Stoppa *et al.* (2003)
Lugiin Gol, Mongolia	Nepheline syenite–fluorite–calcite veinlets with pseudo-graphic intergrowths of fluorite and calcite	Kynicky *et al.* (2019)
Mushgai-Khudag, Mongolia	Quartz-fluorite, fluorite–apatite-celestine, fluorite–calcite rocks	Redina *et al.* (2020)
Arshan, Yuzhnoe, and Ulan-Ude, Russia	Fluorite-rich rocks	Redina *et al.* (2021)

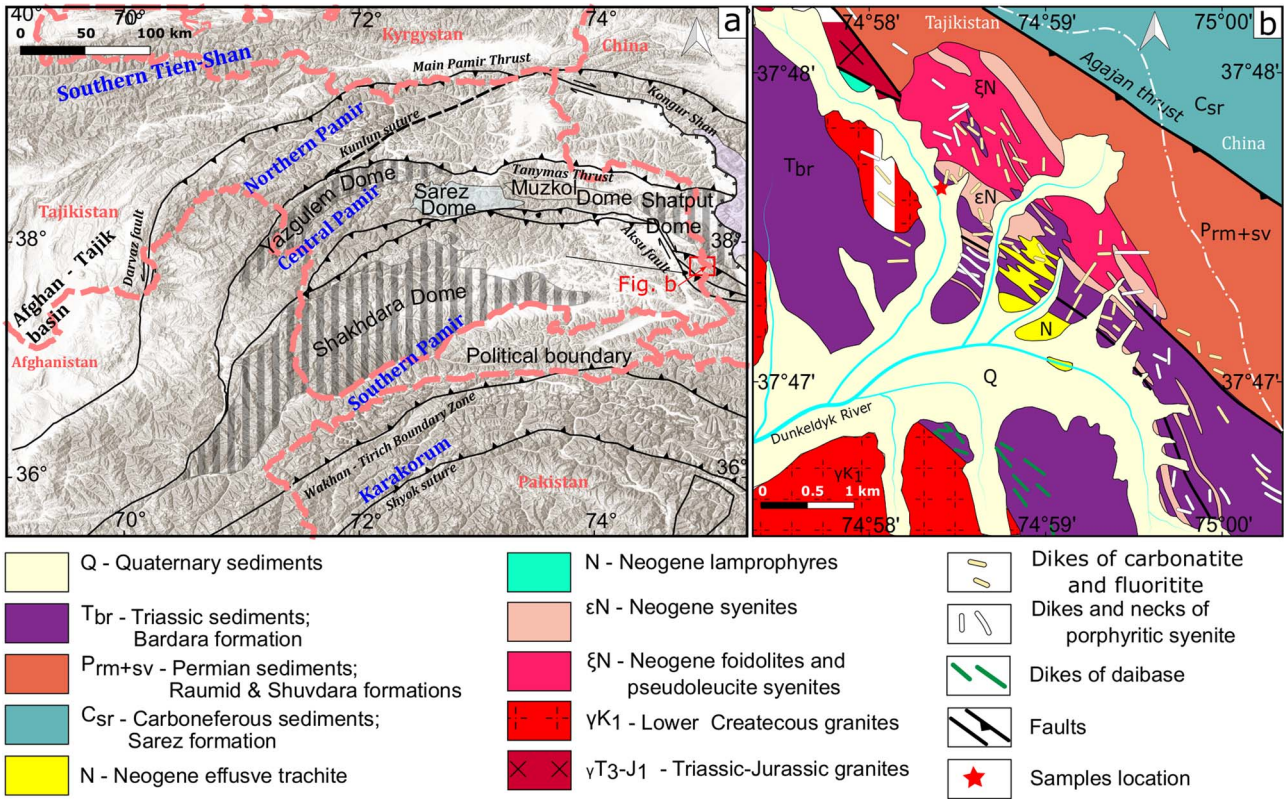

Fig. 1. (A) Tectonic map of the Pamir orogen with outlines of gneiss domes and the study area and (B) Geological map of the Dunkeldyk area, modified after Dmitriev (1976). The investigated outcrop is located 37°47′59.9″N, 74°58′11.64″E.

orogenic collapse and deep crustal exhumation, which produced the metamorphic core complexes with anatectic granites in the center (Stubner *et al.*, 2013).

The Dunkeldyk area is located in the south-eastern part of the Pamir plateau of Tajikistan, on the western slopes of Sarykol mountain range, which marks the border between Tajikistan and China, in the upper reaches of the Dunkeldyk river, a tributary of the Aksu (Fig. 1A). The Dunkeldyk alkaline province is represented by the fractionated Verhne-Dunkeldyk alkaline intrusion and abundant dikes, pipes, and volcanic tuffs of alkaline rocks and carbonatites (Fig. 1B; Dmitriev, 1976; Faiziev *et al.*, 2000). The magmatism of the province started with leucite-bearing rocks and was followed by syenites, quartz trachytes, and carbonatites (Faiziev *et al.*, 2000). The Dunkeldyk fluorite-bearing carbonatites and syenites yielded U–Pb zircon ages of 10.3–10.8 Ma (Hong *et al.*, 2019; Li & Liu, 2023), which are similar to the ages of the Taxkorgan intrusive complex (10.3–11.5 Ma), located east of Dunkeldyk in China (Tang *et al.*, 2022). The mid-Miocene alkaline magmatism in the Southern Pamir has been attributed to crustal shortening and the foundering of the lower crust into the mantle (Shaffer *et al.*, 2017).

The dikes of carbonate and fluorite-rich rocks have been observed on the eastern flank of the upper reaches of the Dunkeldyk valley, whereas boulders of similar rocks were found on the western flank and in the alluvial deposits. The dikes are hosted by the dark, fine-grained metasedimentary rocks of the Triassic Bardara Formation (Fig. 2A). Dikes vary in thickness from 30 to 60 cm and dip at 30 to 60°. The contacts of the dikes with the host are sharp and linear (Fig. 2A, B). Occasionally, the host rocks are brecciated and cemented by quartz-fluorite stockworks with

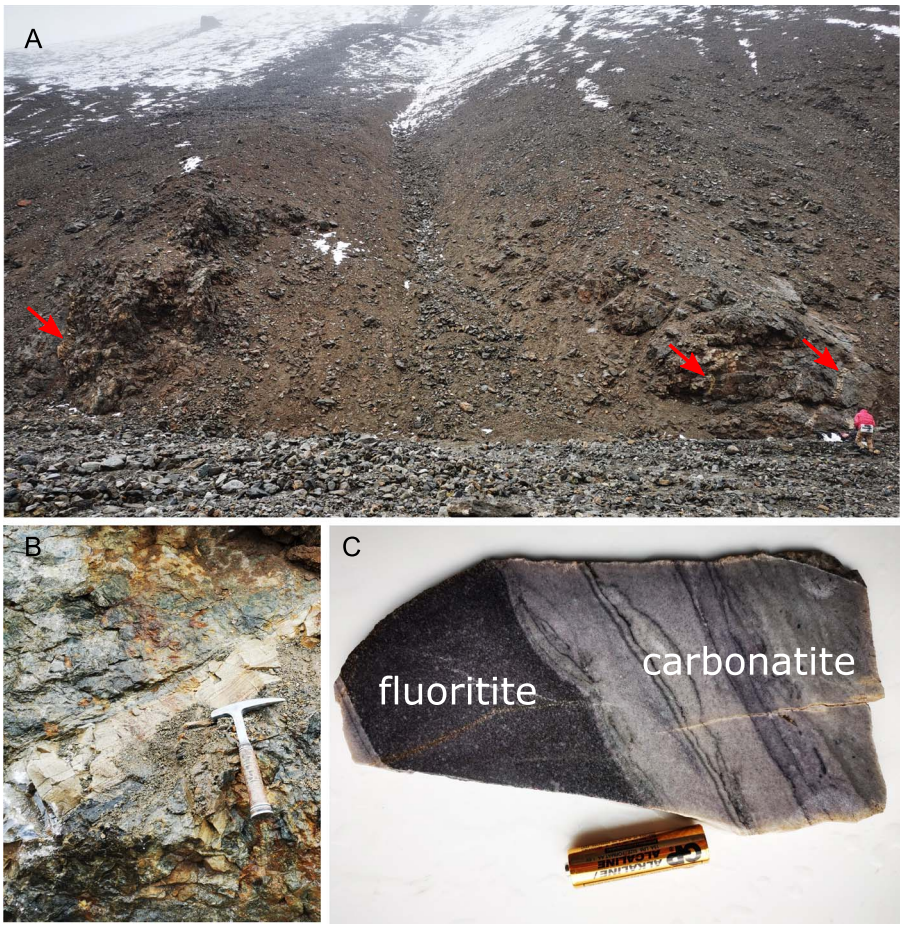

Fig. 2. Geologic relations of Dunkeldyk carbonatite-fluoritite dikes. (A) The field photo of the dikes outcrop. A person is for scale. (B) The carbonatite-fluoritite dike with clear contact and layering. (C) The internal structure of the dike sample.

sulfides; otherwise, visible alteration in the vicinity of the dikes is absent. For this study, four different dikes have been sampled and lump samples were collected from the alluvium.

ROCK TEXTURES AND MINERAL CHEMISTRY

The dikes show layering parallel to the host contacts, with boundaries varying from sharp to gradual and diffuse (Fig. 2B, C). The layering is caused by the differentiation of the light layers enriched in calcite and the dark layers with fluorite and sulfides (Fig. 2B, C). The dikes margins show zonation with a layer of calcite carbonatite at the contact, sometimes with skeletal calcite clouded by fluorite micro inclusions growing in the direction of the dike center followed by coarser fluorite (Fig. 3A). The dike central parts have textures from equigranular to weakly porphyritic (Fig. 3B–D). The mineralogy is diverse and represented by calcite and fluorite, with sulfate (celestine-baritocelestine-barite), phosphate (apatite), sulfides (pyrite, sphalerite, chalcopyrite and galena), REE fluorcarbonates and minor silicates (quartz and biotite). The rocks are dense, have low porosity and low oxidation/weathering, indicated only by the presence of oxides wulfenite ($PbMoO_4$) and plattnerite (PbO_2).

Calcite ranges from skeletal to fine-medium-grained, often elongated crystals in the groundmass of calcite-rich rocks and interstitial grains in fluorite-rich rocks (Fig. 3A–F). Calcite contains up to 0.3 wt% MgO, ~0.2 wt% MnO, 0.4–2.0 wt% FeO, and 0.2–1.0 wt% SrO (Supplementary Table S3). Fluorite grains are isometric, generally anhedral, range from ultra-fine to 1–2 mm in size (Fig. 3) and either dispersed in calcite or concentrated in bands (Fig. 3). The significant impurity in fluorite is Sr reaching 2.1 wt% (Supplementary Table S3). The cathodoluminescence images (CL) of fluorite revealed rounded blue zonation of some grains (Fig. 3B). The Ba-Sr sulfates form irregular grains and range from barite to celestine with the majority of analyses showing 62–88% of celestine (Supplementary Table S3). Sulfides are disseminated in the rocks and mostly represented by pyrite (Fig. 3C).

In addition to dike samples, a coarse-grained fluorite–apatite rock was investigated. Fluorite accounts for >70 wt% of the rock and euhedral prismatic apatite forms ~15 wt%, whereas minor quartz, biotite, and calcite occur in interstices between fluorite and apatite. Apatite hosts rounded inclusions of fluorite (Fig. 3E), similar to fluorite zonation in carbonatite samples (Fig. 3B). Apatite contains 14–15 wt% of total rare earth oxides (TREO), which correlate with 7.7–8.2 wt% SiO_2 (Fig. 4), and 2.4–3.1 wt% SO_3 (Supplementary Table S3). Apatite shows alteration to the secondary low-REE apatite containing <2 wt% TREO and 0.2–0.6 wt% Na_2O with fine-grained inclusions of REE fluorcarbonates (parisite and synchysite), formed by dissolution–precipitation replacement of the primary apatite (Fig. 3F). The purple coloration of fluorite contacting altered/recrystallized apatite could be due to U and Th released by alteration (Fig. 3E).

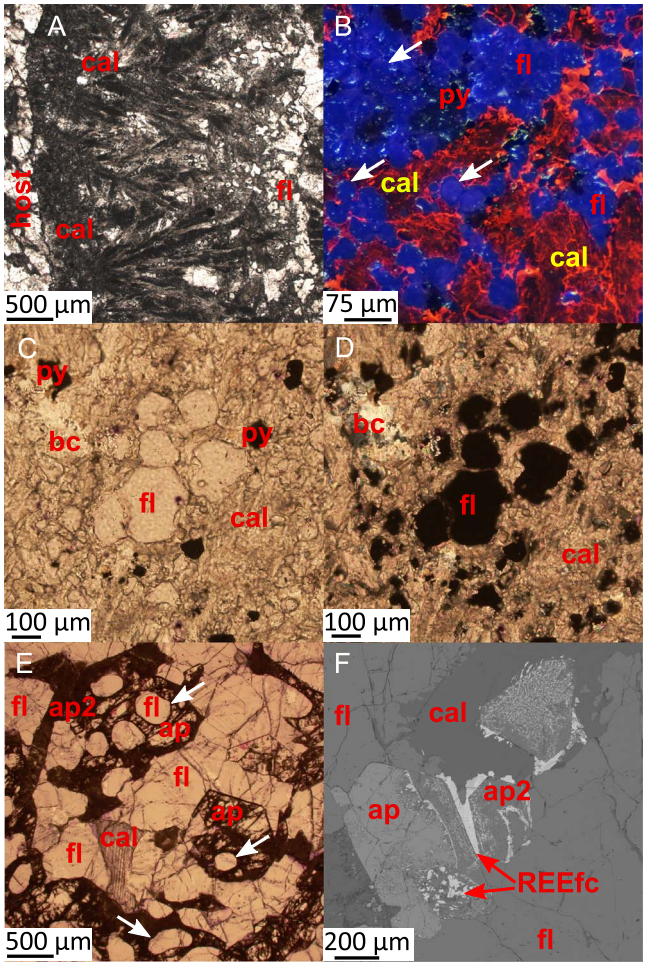

Fig. 3. Mineralogy and petrography of carbonatite-fluoritites. (A) Skeletal feathery crystals of calcite grew from the contact with the host rock to dike center. Fluorite forms micro inclusions in calcite, resulting in cloudy calcite appearance, and larger fluorite crystals concentrated closer to the dike center. (B) Colored CL image of fluoritite, with fluorite highlighted by blue and calcite by red luminescence. Fluorite has rounded brighter blue annular zonation and occasional circular intergrowth with calcite, suggesting that it had spherical crystal shape during early stages of crystallization. Image pair (C; PPL) and (D; XPL) shows the occurrence and morphology of fluorite in the matrix of fine-grained calcite. Sulfides (mostly pyrite) are visible as black grains in PPL and fluorite becomes dark in XPL. Transmitted light (E; PPL) and BSE (F) images of coarse-grained fluorite-apatite rock. Euhedral apatite contains round fluorite inclusions (highlighted by arrows) and calcite occurs in interstices between apatite and fluorite. Primary transparent high-REE apatite is partially altered (F), forming aggregate of low-REE apatite and REE fluorcarbonates. The release or radioactive elements (U and Th) by alteration likely is responsible for deep purple coloration of fluorite adjacent to altered apatite. Minerals include fluorite (fl), calcite (cal), baritocelestine (bc), pyrite (py), apatite (ap), and REE fluorcarbonates (REEfc).

GEOCHEMISTRY

The bulk rock composition was determined by a combination of energy dispersive spectroscopy, X-ray fluorescence, and ICP-MS (Table 2; Supplementary Tables S2 and S3). The samples range from calcite carbonatites with high fluorite content to fluorite-dominated rocks (Fig. 4A). Due to the predominance of the F anion, the fluorite-rich rocks have anomalously low content of O. The cations are dominated by Ca ranging from 29.2 to 36.4 wt%. The Sr and Ba content is high and variable, reaching 4.7 wt% Ba and 7.1 wt% Sr. The content of Si, Al, and Ti is <2 wt% in all rock varieties, while Na is close to the detection limit of 0.03 wt% and K < 1 wt%. Celestine-barite, together with pyrite, hosts 0.3–4.4 wt% S. The fluorite-rich rocks have an elevated P content, reaching 3.4 wt% P in apatite-fluorite rock, while carbonatites contain <0.4 wt% P. Elevated concentrations were observed for base metals (Pb and Zn) and > 3 wt% TREO in fluorite-apatite rock (Table 2). The rocks have LREE-enriched patterns with 6–20 times the upper crustal average (Fig. 4B), and the Y/Ho ranges from 28 to 47, with average 41.

DISCUSSION

Magmatic origin of carbonate-fluorite rocks

Dunkeldyk carbonate-rich rocks contain REE fluorcarbonates, which are characteristic for carbonatites (Nikolenko *et al.*, 2022). Carbonatite compositions show high content of Ba, Sr, and REE, which are characteristic for magmatic carbonate rocks (Stoppa *et al.*, 2023). Because of the magmatic origin of carbonatites, the intricate association with fluorite-rich rocks and mineralogy suggests the magmatic origin of the Dunkeldyk fluorite-rich rocks. The fluorite inclusions in apatite and calcite have a round shape and circular CL zonation (Fig. 3D, E). Spherical shape is characteristic for fluorite produced in magmatic crystallization experiments (Veksler *et al.*, 2005; Chebotarev *et al.*, 2018) and was attributed to minimal surface energy of this crystal shape (Veksler *et al.*, 2005). While both calcite and fluorite are common hydrothermal minerals, the textures of Dunkeldyk rocks are distinctively different from the hydrothermal veins, where drusy aggregates and cubic/octahedral oscillatory zoning are typical for hydrothermal fluorite (Schwinn & Markl, 2005; Barker *et al.*, 2009).

The key parameter of the magmatic process is temperature. Dolejs (2005) argued that fluorite melt is unlikely to form in nature because of very high melting temperature of fluorite (1418°C). Carbonate reduces the fluorite solidus dramatically, and the system of $CaCO_3$–CaF_2 has eutectic at 880°C and 36 wt% CaF_2 and 64 wt% $CaCO_3$ (Gittins & Tuttle, 1964). The presence of components such as sulfates, sulfides and water, likely additionally suppressed the crystallization temperatures of melts; however, the low porosity and absence of explosive and brecciated textures argue against large-scale fluid exsolution during crystallization. In fluorite–apatite rocks, primary apatite with 14–15 wt% TREO, LREE-enriched patterns, and britholite-type substitution (Fig. 4C), which is characteristic for magmatic apatite (Stepanov *et al.*, 2023), decomposed to REE fluorcarbonates and low-REE apatite, typical for subsolidus replacement. The primary apatite has a composition similar to apatite synthesized with britholite at 800°C in melt crystallization experiments (Stepanov *et al.*, 2023). Calcite from carbonatite has a high REE content (~4000 ppm REE) measured by LA-ICP-MS and REE patterns parallel to apatite (Fig. 4D). The significant content of Mn, Sr, and REE-enriched patterns are typical for magmatic calcite (Vichi *et al.*, 2005; Chakhmouradian *et al.*, 2016; Ying *et al.*, 2020). Considering that fluoritites are found in multiple localities of Dunkeldyk (Supplementary Fig. S1) and the diversity of fluoritite textures, it is likely that rocks have formed over a range of temperatures 600–800°C. Our observations reaffirm the conclusion of Dolejs (2005) that pure fluorite melts are unlikely to occur in nature; however, the much lower temperature of melts close to fluorite–calcite eutectics is favorable for the formation of fluorite-dominated othomagmatic rocks (Kynicky *et al.*, 2019).

The compositions of Dunkeldyk rocks are remarkably similar to the rocks of Central Italy (Table 2; Stoppa *et al.*, 2016), which could be another evidence for the similarity of their origin. The term fluoritite has occasionally been used for volcanic rocks in Italy

Table 2: Whole rock compositions of carbonatites and fluoritites from Dunkeldyk

Sample	22T50a	22T53a	22T52xb	22T56b	22T56a	22T51SH	21 T98	22T51ab	22T52xa	22T51Y	22T51aa	PIA03*
Si (wt%)	0.48	1.52	0.36	0.74	0.02	0.14	1.96	0.88	0.89	0.20	0.71	2.32
Al	0.14	0.45	0.09	0.05	<0.01	0.03	0.05	0.18	0.17	0.03	0.17	1.05
Ti	0.006	0.023	0.011	0.008	0.007	0.006	0.015	0.017	0.016	0.005	0.017	0.05
Fe	0.38	0.78	0.57	0.62	0.71	0.53	0.62	2.96	2.82	0.52	0.69	1.33
Mn	0.06	0.08	0.10	0.15	0.12	0.10	0.02	0.07	0.08	0.08	0.15	0.18
Mg	0.05	0.19	0.20	0.40	0.04	0.13	0.03	0.46	0.46	0.14	0.28	0.20
Ca	31.9	31.6	31.6	29.2	31.3	32.9	36.4	32.7	30.6	33.1	34.1	40.09
Na	0.02	0.04	0.02	0.02	0.01	0.02	0.06	0.03	0.03	0.02	0.02	0.18
K	0.18	0.59	0.15	0.20	0.01	0.06	0.01	0.35	0.33	0.08	0.29	0.19
Ba	3.33	0.90	2.11	4.72	2.71	0.75	0.02	1.31	1.29	0.72	1.03	9.39
Sr	5.7	6.0	6.1	6.6	6.6	6.8	0.1	3.2	2.9	6.7	4.3	0.29
P	0.06	0.10	0.09	0.21	0.37	0.08	3.39	0.38	0.37	0.07	0.17	0.170
S	1.94	2.25	2.25	2.16	2.60	2.21	0.29	4.38	4.13	2.17	1.72	0.48
F	14.1	12.0	12.1	14.5	13.6	13.0	32.3	25.2	25.0	13.1	13.5	28.8
O	24.18	24.20	25.85	21.33	23.30	25.85	9.15	12.66	10.33	26.01	27.40	
C	5.54	6.05	6.02	4.62	5.50	6.15	1.71	2.62	2.05	6.18	6.37	0.11
Cu (ppm)	15.8	15.9	13.8	59.8	6.9	10.5	1.5	89.0	89.9	3.7	31.5	4.0
Zn	126	311	274	328	118	289	18	1050	936	141	300	54
Pb	1925	1570	1030	750	827	1100	31	5400	4200	993	1160	636
V	35	44	56	80	21	31	107	144	140	34	53	310
Ga	1.0	3.0	2.2	1.4	0.6	1.2	9.7	3.1	2.8	1.4	2.3	NA
Cr	<10	<10	<10	<10	<10	<10	<10	<10	<10	<10	<10	23
Y	33	43	27	34	17	47	888	52	49	45	46	16
La	422	1020	1275	1115	1125	1270	10 902	1140	1240	1370	892	195
Ce	428	1395	1470	1195	1370	1700	17 464	1750	1805	1825	1210	170
Pr	26.4	110.0	102.5	73.1	90.2	132.0	1632	142.5	148.5	139.0	94.8	NA
Nd	68.4	321	273	177.5	214	372	5160	439	424	389	274	30
Sm	7.40	33.5	24.6	13.10	14.15	38.8	624	47.5	44.9	39.1	30.8	1.0
Eu	2.10	6.69	4.98	2.64	2.47	7.84	122.5	9.28	8.96	7.63	6.01	0.50
Gd	5.29	15.95	10.60	7.16	5.17	18.15	333	21.2	20.5	17.45	14.60	NA
Tb	0.88	1.72	1.16	1.17	0.66	1.96	37.9	2.22	2.10	1.86	1.61	<0.1
Dy	4.66	6.55	3.94	6.11	2.70	7.44	158.5	8.28	7.74	6.90	6.48	NA
Ho	0.84	1.02	0.58	1.22	0.47	1.12	25.6	1.19	1.09	1.04	0.98	NA
Er	2.10	2.20	1.11	3.11	1.14	2.47	59.4	2.50	2.32	2.15	2.22	NA
Tm	0.29	0.26	0.14	0.43	0.17	0.30	7.59	0.30	0.28	0.27	0.28	NA
Yb	1.58	1.43	0.75	2.58	0.97	1.61	39.7	1.70	1.52	1.49	1.63	<0.05
Lu	0.19	0.19	0.10	0.34	0.13	0.22	5.12	0.21	0.20	0.21	0.22	<0.01
Th	9.35	17.15	7.98	34.8	49.3	13.25	781	107.0	106.5	11.00	24.3	7
U	2.00	12.55	11.95	15.50	17.75	22.5	276	19.20	19.65	10.55	59.1	22
Nb	1.3	13.4	14.2	1.0	3.8	18.6	4.8	25.1	25.6	10.6	64.1	52
Ta	<0.05	0.08	<0.05	<0.05	<0.05	<0.05	0.07	0.11	0.10	<0.05	<0.05	<0.3
REE	981	2945	3188	2649	2894	3590	37 629	3692	3833	3823	2619	>396
Total (wt%)	100.6	98.1	100.8	97.8	99.5	101.7	98.9	98.2	91.0	102.0	103.8	96.6
Fluorite	31.0	27.0	26.7	33.2	29.9	28.0	81.4	58.2	62.1	28.2	29.4	
Calcite	52.3	58.7	57.3	46.2	51.9	57.1	18.5	26.9	22.9	57.3	60.0	
Sulfate	16.6	14.4	16.1	20.7	18.2	14.8	0.1	14.9	15.0	14.5	10.6	

*denotes composition of 'carbothermal residua' from Stoppa *et al.* (2016). NA, not analyzed.

(Stoppa *et al.*, 2016) and in Mushgai Khudak, a rare metal deposit in Mongolia (Redina *et al.*, 2020). Fluoritite seems to be the most suitable name for Dunkeldyk rocks with >50% fluorite.

Crystallization mechanisms

The Dunkeldyk rocks show a wide range of textures, suggesting different mechanisms of crystallization. The skeletal spinifex-like texture of the dike margin (Fig. 3A) indicates heterogeneous nucleation and fast crystallization from a quickly cooling melt. The textures with disseminated euhedral crystals observed in the majority of samples (Fig. 3B, C) are typical for homogeneous nucleation in melts with moderate supersaturation (London, 2005).

The characteristic feature of Dunkeldyk dikes is the layering of carbonatite and fluoritite (Fig. 2). The delineation of the layers parallel to the host suggests that both carbonatites and fluoritites have originated from the same magma. Gravity settling was unlikely to play a role as the layering is parallel to the host contact and rather symmetrical. The projection to calcite–fluorite mixtures plots carbonatites close to CaF_2-$CaCO_3$ eutectic (Fig. 4A). The fluoritites fluorite content is significantly higher than CaF_2-$CaCO_3$ eutectic, which suggests melt oversaturation in fluorite and/or concentration during crystallization. Differentiation by sequential nucleation of rock-forming minerals, similar to the mechanism of layered aplite crystallization by London (2005) can explain layered structure. The fast cooling of the melt caused immediate nucleation and crystallization of calcite, which resulted in the development of a boundary melt layer enriched in fluoride, forming fluoritite. The fluorite–apatite rocks possibly formed from a larger melt volume, where gravity settling of dense

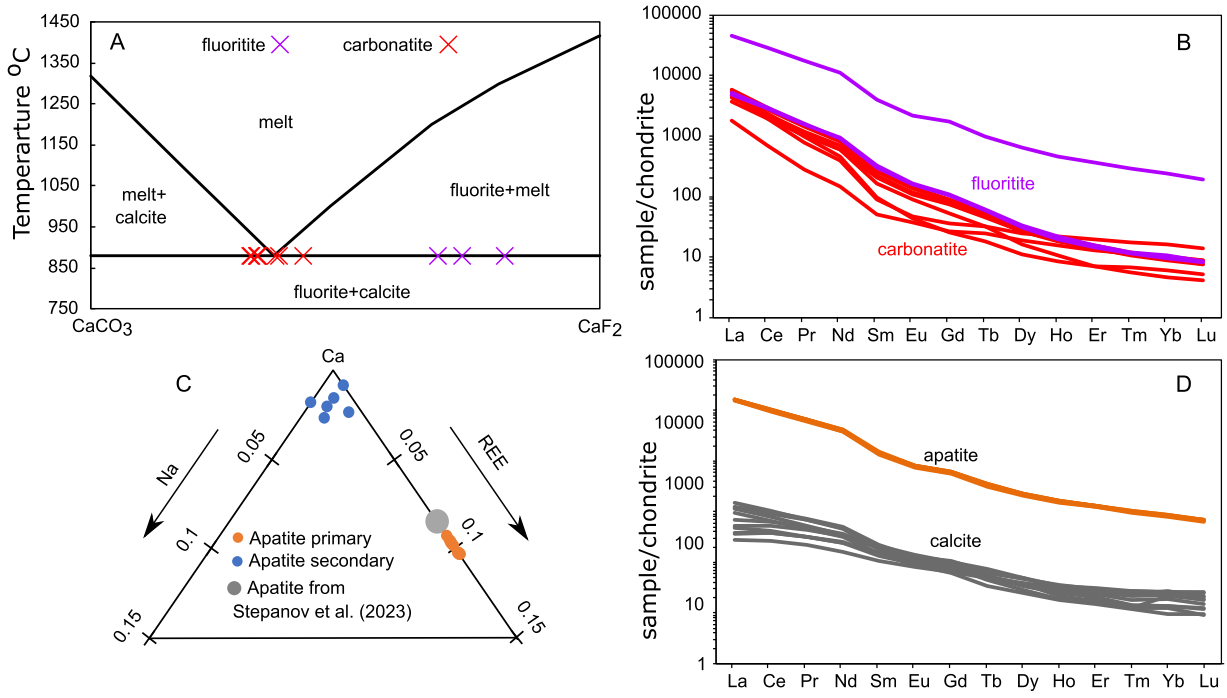

Fig. 4. Key chemical characteristics of the Dunkeldyk carbonatite–fluoritites. (A) The anhydrous CaF_2-$CaCO_3$ phase diagram at 0.1 GPa based on Gittins & Tuttle (1964). The projection of the rocks to calcite-fluorite joint is shown. (B) Bulk rock REE patterns normalized to chondrite. (C) Projection of apatite composition on a ternary Na-Ca-REE plot. The experimental REE-saturated apatite from Stepanov *et al.* (2023) marks the REE solubility in apatite at 800°C. (D) REE patterns of Dunkeldyk calcite and apatite normalized to chondrite (McDonough & Sun, 1995).

apatite and fluorite resulted in the formation of fluoritite–apatite cumulates.

Petrogenesis of Dunkeldyk carbonatites and fluoritites

The carbonatite dikes show clear association with alkaline rocks of Verhne-Dunkeldyk intrusion (Dmitriev, 1976; Faiziev *et al.*, 2000). The absence of voluminous mafic magmatism and low Mg of Dunkeldyk carbonatites precludes the formation of these rocks by mantle melting (Hong *et al.*, 2019). Dunkeldyk samples show elevated Y/Ho, with average 41, higher than upper crustal Y/Ho of 25 (Rudnick & Gao, 2003). Enrichment of Y relative to Ho is consistent with preferential partitioning of Y to fluoride melt observed in experiments by Veksler *et al.* (2005) and provide evidence for the formation of Dunkeldyk carbonatite–fluoritites by miscibility from silicate melt.

Molten salts with the same cation and different anions show near ideal behavior and complete solubility (Treiman, 1995). Therefore, most carbonatites likely were fluorite undersaturated during crystallization (Fig. 4A; Stoppa *et al.*, 2023), and crystallization of carbonates concentrated F in the residual liquid. If calcite–fluorite (eu-)cotectic could be reached then high-fluorite carbonatites with eutectic proportion form. Gravity and crystallization fractionation of fluorite from such melts produce fluorite-dominated rocks: fluoritites.

A number of studies proposed that fluoride melts could play an important role in transport and concentration of metals (Veksler *et al.*, 2012; Vasyukova & Williams-Jones, 2016; Kynicky *et al.*, 2019). The experiments have demonstrated high solubility of REE and Nb in carbonatite–fluoride melts (Chebotarev *et al.*, 2018). The rocks described in this study contain abundant accessory sulfides, consistent with association of base metal mineralization with fluoritites in Dunkeldyk area (Faiziev *et al.*, 2000). Similarly, carbonate–fluorite rocks from Mongolia showed association with abundant sulfides (Kynicky *et al.*, 2019). The fluorite–apatite rock has a significant content of P and ~3 wt% TREO. All this evidence points to high capacity of fluoride melts to concentrate and transport a wide range of economically important metals. Fluorite-rich rocks have been observed in carbonatite-associated REE deposits in Bayan Obo, Maoniuping, and Daluxiang in China (Xu *et al.*, 2008), Eldor carbonatite in Canada (Beland & Williams-Jones, 2021) and other mineral deposits. Carbonatites and especially those in large deposits have complex magmatic and postmagmatic evolution, obscuring primary textures. Future studies will investigate the origin of fluoritites in those deposits; however, Dunkeldyk fluoritites suggest that crystallization from carbonate-fluoride melts should be considered.

Data availability

The data underlying this article are available in the article and in its online supplementary material.

Supplementary Data

Supplementary data are available at *Journal of Petrology* online.

Acknowledgements

Willy Williams-Jones is acknowledged for his encouragement and insightful comment on the manuscript, and Francesco Stoppa and anonymous reviewers are thanked for valuable suggestions. Ma Ying is thanked for assistance with CL image collection. Denis Mikhailenko assisted during the field work and Andrey Korsakov helped with sample preparation. The study was financially supported by the National Natural Science Foundation of China (grant no. 92162323).

References

Aminov, J., Ding, L., Mamadjonov, Y., Dupont-Nivet, G., Aminov, J., Zhang, L.-Y., Yoqubov, S., Aminov, J. & Abdulov, S. (2017). Pamir plateau formation and crustal thickening before the India-Asia collision inferred from dating and petrology of the 110–92Ma southern Pamir volcanic sequence. *Gondwana Research* **51**, 310–326. https://doi.org/10.1016/j.gr.2017.08.003.

Angiolini, L., Zanchi, A., Zanchetta, S., Nicora, A. & Vezzoli, G. (2013). The Cimmerian geopuzzle: new data from south Pamir. *Terra Nova* **25**, 352–360. https://doi.org/10.1111/ter.12042.

Barker, S. L. L., Bennett, V. C., Cox, S. F., Norman, M. D. & Gagan, M. K. (2009). Sm–Nd, Sr, C and O isotope systematics in hydrothermal calcite–fluorite veins: implications for fluid–rock reaction and geochronology. *Chemical Geology* **268**, 58–66. https://doi.org/10.1016/j.chemgeo.2009.07.009.

Beland, C. M. J. & Williams-Jones, A. E. (2021). The genesis of the Ashram REE deposit, Quebec: insights from bulk-rock geochemistry, apatite-monazite-bastnäsite replacement reactions and mineral chemistry. *Chemical Geology* **578**, 120298. https://doi.org/10.1016/j.chemgeo.2021.120298.

Chakhmouradian, A. R., Reguir, E. P., Couëslan, C. & Yang, P. (2016). Calcite and dolomite in intrusive carbonatites II. Trace-element variations. *Mineralogy and Petrology* **110**, 361–377. https://doi.org/10.1007/s00710-015-0392-4.

Chapman, J. B., Scoggin, S. H., Kapp, P., Carrapa, B., Ducea, M. N., Worthington, J., Oimahmadov, I. & Gadoev, M. (2018). Mesozoic to cenozoic magmatic history of the Pamir. *Earth and Planetary Science Letters* **482**, 181–192. https://doi.org/10.1016/j.epsl.2017.10.041.

Chebotarev, D. A., Veksler, I. V., Wohlgemuth-Ueberwasser, C., Doroshkevich, A. G. & Koch-Müller, M. (2018). Experimental study of trace element distribution between calcite, fluorite and carbonatitic melt in the system CaCO3 + CaF2 + Na2CO3 ± Ca3(PO4)2 at 100 MPa. *Contributions to Mineralogy and Petrology* **174**, 4.

Dmitriev, E. A. (1976) *Cenozoic potassium alkaline rocks of the Eastern Pamirs*. Dushanbe, (in Russian).

Dolejs, D. (2005). Evidence for fluoride melts in Earth's mantle formed by liquid immiscibility: comment. *Geology* **33**, e76. https://doi.org/10.1130/0091-7613-33.1.e76.

Faiziev, A. R., Iskandarov, F. S. & Gafurov, F. G. (2000) *Mineralogy, thermobarogeochemcial conditions and genesis of REE-fluorite deposit Dunkeldyk (Eastern Pamir)*. Dushanbe (in Russian): Khumo.

Gittins, J. & Tuttle, O. F. (1964). The system CaF2 - Ca(OH)2 -CaCO3. *American Journal of Science* **262**, 66–75. https://doi.org/10.2475/ajs.262.1.66.

Hong, J., Ji, W., Yang, X., Khan, T., Wang, R., Li, W. & Zhang, H. (2019). Origin of a Miocene alkaline–carbonatite complex in the Dunkeldyk area of Pamir, Tajikistan: petrology, geochemistry, LA–ICP–MS zircon U–Pb dating, and Hf isotope analysis. *Ore Geology Reviews* **107**, 820–836. https://doi.org/10.1016/j.oregeorev.2019.03.009.

Kynicky, J., Smith, M. P., Song, W., Chakhmouradian, A. R., Xu, C., Kopriva, A., Galiova, M. V. & Brtnicky, M. (2019). The role of carbonate-fluoride melt immiscibility in shallow REE deposit evolution. *Geoscience Frontiers* **10**, 527–537. https://doi.org/10.1016/j.gsf.2018.02.005.

Lentz, D. (1991). Radioelement distribution in U, Th, Mo, and rare-earth-element pegmatites, skarns, and veins in a portion of the Grenville Province, Ontario and Quebec. *Canadian Journal of Earth Sciences* **28**, 1–12. https://doi.org/10.1139/e91-001.

Li, Z. & Liu, Y. (2023). Crust–mantle interaction beneath the Pamir orogenic belt: insights from the Miocene Dunkeldyk carbonatite–syenite complex in Tajikistan. *Ore Geology Reviews* **157**, 105411. https://doi.org/10.1016/j.oregeorev.2023.105411.

London, D. (2005). Granitic pegmatites: an assessment of current concepts and directions for the future. *Lithos* **80**, 281–303. https://doi.org/10.1016/j.lithos.2004.02.009.

McDonough, W. & Sun, S. (1995). The composition of the earth. *Chemical Geology* **120**, 223–253. https://doi.org/10.1016/0009-2541(94)00140-4.

Nikolenko, A. M., Stepanov, K. M., Roddatis, V. & Veksler, I. V. (2022). Crystallization of bastnäsite and burbankite from carbonatite melt in the system La(CO3)F-CaCO3-Na2CO3 at 100 MPa. *American Mineralogist* **107**, 2242–2250. https://doi.org/10.2138/am-2022-8064.

Peretyazhko, I. S., Zagorsky, V. Y., Tsareva, E. A. & Sapozhnikov, A. N. (2007). Immiscibility of calcium fluoride and aluminosilicate melts in ongonite from the Ary-Bulak intrusion, eastern Transbaikal region. *Doklady Earth Sciences* **413**, 315–320. https://doi.org/10.1134/S1028334X07020419.

Redina, A. A., Nikolenko, A. M., Doroshkevich, A. G., Prokopyev, I. R., Wohlgemuth-Ueberwasser, C. & Vladykin, N. V. (2020). Conditions for the crystallization of fluorite in the Mushgai-Khudag complex (southern Mongolia): evidence from trace element geochemistry and fluid inclusions. *Geochemistry* **80**, 125666. https://doi.org/10.1016/j.chemer.2020.125666.

Redina, A. A., Doroshkevich, A. G., Veksler, I. V. & Wohlgemuth-Ueberwasser, C. C. (2021). Fluorite mineralization related to Carbonatitic magmatism in the Western Transbaikalia: insights from fluid inclusions and trace element composition. *Minerals* **11**, 1183. https://doi.org/10.3390/min11111183.

Rudnick, R. L. & Gao, S. (2003). Composition of the Continental Crust. In: Holland, H. D. & Turekian, K. K. (eds) *Treatise on Geochemistry*. Oxford: Elsevier, 1–64, https://doi.org/10.1016/B0-08-043751-6/03016-4.

Schwinn, G. & Markl, G. (2005). REE systematics in hydrothermal fluorite. *Chemical Geology* **216**, 225–248. https://doi.org/10.1016/j.chemgeo.2004.11.012.

Shaffer, M., Hacker, B. R., Ratschbacher, L. & Kylander-Clark, A. R. C. (2017). Foundering triggered by the collision of India and Asia captured in xenoliths. *Tectonics* **36**, 1913–1933. https://doi.org/10.1002/2017TC004704.

Stepanov, A. S., Zhukova, I. A. & Jiang, S.-Y. (2023). Experimental constraints on miscibility gap between apatite and britholite and REE partitioning in an alkaline melt. *American Mineralogist* **108**, 1043–1052. https://doi.org/10.2138/am-2022-8535.

Stoppa, F., Rosatelli, G., Wall, P. & Michael, J. (2003) *Texture and mineralogy of tuffs and tuffisites at Ruri Volcano in western Kenya: a carbonatite, melilitite, mantle-debris trio*. Periodico Di Mineralogia.

Stoppa, F., Pirajno, F., Schiazza, M. & Vladykin, N. V. (2016). State of the art: Italian carbonatites and their potential for critical-metal deposits. *Gondwana Research* **37**, 152–171. https://doi.org/10.1016/j.gr.2016.07.001.

Stoppa, F., Cirilli, S., Sorci, A., Broom-Fendley, S., Principe, C., Perna, M. G. & Rosatelli, G. (2023). Igneous and sedimentary 'limestones': the puzzling challenge of a converging classification. *Geological Society* **520**, 327–352. https://doi.org/10.1144/SP520-2021-120.

Stubner, K. *et al.* (2013). The giant Shakhdara migmatitic gneiss dome, Pamir, India-Asia collision zone: 2. Timing of dome formation. *Tectonics* **32**, 1404–1431.

Tang, G.-J., Wyman, D. A., Wang, Q., Yin, J.-Y. & Dan, W. (2022). Long-distance lateral magma propagation and Pamir

plateau uplift. *Geophysical Research Letters* **49**, e2021GL096467. https://doi.org/10.1029/2021GL096467.

Treiman, A. H. (1995). Ca-rich carbonate melts: a regular-solution model, with applications to carbonatite magma + vapor equilibria and carbonate lavas on Venus. *American Mineralogist* **80**, 115–130. https://doi.org/10.2138/am-1995-1-212.

Vasyukova, O. & Williams-Jones, A. E. (2016). The evolution of immiscible silicate and fluoride melts: implications for REE ore-genesis. *Geochimica et Cosmochimica Acta* **172**, 205–224. https://doi.org/10.1016/j.gca.2015.09.018.

Veksler, I. V., Dorfman, A. M., Kamenetsky, M., Dulski, P. & Dingwell, D. B. (2005). Partitioning of lanthanides and Y between immiscible silicate and fluoride melts, fluorite and cryolite and the origin of the lanthanide tetrad effect in igneous rocks. *Geochimica et Cosmochimica Acta* **69**, 2847–2860. https://doi.org/10.1016/j.gca.2004.08.007.

Veksler, I. V., Dorfman, A. M., Dulski, P., Kamenetsky, V. S., Danyushevsky, L. V., Jeffries, T. & Dingwell, D. B. (2012). Partitioning of elements between silicate melt and immiscible fluoride, chloride, carbonate, phosphate and sulfate melts, with implications to the origin of natrocarbonatite. *Geochimica et Cosmochimica Acta* **79**, 20–40. https://doi.org/10.1016/j.gca.2011.11.035.

Vichi, G., Stoppa, F. & Wall, F. (2005). The carbonate fraction in carbonatitic Italian lamprophyres. *Lithos* **85**, 154–170. https://doi.org/10.1016/j.lithos.2005.03.025.

Xu, C., Campbell, I. H., Kynicky, J., Allen, C. M., Chen, Y., Huang, Z. & Qi, L. (2008). Comparison of the Daluxiang and Maoniuping carbonatitic REE deposits with Bayan obo REE deposit, China. *Lithos* **106**, 12–24. https://doi.org/10.1016/j.lithos.2008.06.005.

Yang, L. & van Hinsberg, V. J. (2019). Liquid immiscibility in the CaF2-granite system and trace element partitioning between the immiscible liquids. *Chemical Geology* **511**, 28–41. https://doi.org/10.1016/j.chemgeo.2019.02.017.

Ying, Y.-C., Chen, W., Simonetti, A., Jiang, S.-Y. & Zhao, K.-D. (2020). Significance of hydrothermal reworking for REE mineralization associated with carbonatite: constraints from in situ trace element and C-Sr isotope study of calcite and apatite from the Miaoya carbonatite complex (China). *Geochimica et Cosmochimica Acta* **280**, 340–359. https://doi.org/10.1016/j.gca.2020.04.028.

Yogibekov, D., Sang, M., Xiao, W., Mamadjonov, Y., Zhou, C., Yang, H., Mao, Q., Aminov, J., Khalimov, G. & Ashuraliev, S. (2023). Post-collisional magmatism associated with the final closure of the Rushan-Pshart Meso-Tethys Ocean in Pamir, Tajikistan: inference from Cretaceous igneous rocks of the Pshart accretionary complex. *Frontiers in Earth Science* **10**. https://doi.org/10.3389/feart.2022.1090952.